

A Hybrid Multi-reference Subband Control Strategy for Active Noise Control Headphones

Vinal Patel^{a,*}, Jordan Cheer^b

^a*Department of Information Technology, ABV-Indian Institute of Information Technology and Management, Gwalior-474015, India*

^b*Institute of Sound and Vibration Research (ISVR), University of Southampton, Southampton SO17 1BJ, United Kingdom*

Abstract

Multi-reference feedforward Active Noise Control (ANC) has been shown to provide increased noise mitigation capability in ANC headphones compared to a single reference feedforward controllers, due to the availability of additional time advanced information. Recent studies have also shown that the integration of a single-reference feedforward controller and a feedback controller increases both the noise cancellation bandwidth and system stability, therefore, a corresponding hybrid version of the multi-reference control strategy has been developed and is presented in this paper. The hybrid multi-reference ANC (HMRANC) system is comprised of a multi-reference feedforward control unit acting in conjunction with a feedback ANC system. In addition, to overcome the high computational demand of the hybrid structure, a delayless subband version of the HMRANC system is also presented in this paper. The proposed HMRANC and delayless subband HMRANC

*Corresponding author, Phone : +919586288218; Fax : +917512449818

Email addresses: vp@iiitm.ac.in (Vinal Patel), j.cheer@soton.ac.uk (Jordan Cheer)

headphone systems achieve an improvement of 5-10 dB over the previously proposed hybrid ANC headphone system for different acoustic field scenarios. Moreover, the delayless subband HMRANC headphone system is 40% less computationally demanding than HMRANC and 10% less demanding than HANC headphone systems.

Keywords: Active noise control, hybrid active noise control, delayless subband adaptive filtering, feedforward systems.

1. Introduction

Acoustical noises degrades both the physiological and psychological health of humans [1]. Therefore, significant effort has been made to develop both active and passive noise reduction techniques that control the noise at the originating source [2]. However, control at source is not always feasible and sometimes it may be more effective and economical to control the noise at the receiving end, i.e., at the human ear. This type of solution typically involves ear defenders, ear plugs, or active noise control (ANC) headphones. Due to the limitations of ear defenders for attenuating low frequency noise, ANC headphones have seen significant commercial success. The most commonly employed strategies for the implementation of ANC in headphones may be classified into either feed-forward, feedback, or hybrid systems. In a feed-forward ANC implementation, a reference microphone is employed to sense the noise disturbance to be attenuated, a loudspeaker is used to generate the necessary anti-noise, and an error microphone is utilized to measure the level of noise cancellation achieved and adapt the controller [3, 4]. Alternatively, in a feedback ANC implementation, the reference signal for ANC is generated

internally and there is no requirement for a physical reference microphone, however, the control bandwidth in this case is generally lower compared to feedforward ANC systems [3, 5].

To increase the stability margin and noise control bandwidth of an ANC system, a combined feedforward-feedback ANC system has been proposed, which is referred to as a Hybrid ANC (HANC) system [6, 7, 8]. Rafaely and Jones developed a HANC system that combines an analog feedback ANC controller and an adaptive digital feedforward ANC controller [8]. In [8, 9] the effect of direct and reverberant sound fields on the noise control performance of a feedforward ANC system is studied, and it was reported that the performance is dependent on the head-set position for direct sound-field scenarios. ~~Theoretical analysis of ANC systems in both time and frequency domains is well investigated to understand the transient and steady-state behaviour of the system under different sound-field conditions~~ [10, 11, 12]. Moreover, it is also reported that the gain margin and system stability of feedforward ANC has been improved by integrating a feedback system component [8, 13, 14, 15].

Recently, a multi-reference control strategy for ANC headphones has been proposed and investigated. This system uses the reference signals from the reference microphones on each ear to improve the performance of the ANC headphones [16, 17, 18]. The main advantage of the multi-reference ANC system over existing ANC headphones strategies is the availability of additional time-advanced information for disturbance sources incident from particular directions, which results in an increased control bandwidth [16, 19]. There remains a potential advantage to include a feedback control component to fur-

ther enhance the noise attenuation capability of the multi-reference strategy for ANC headphones, therefore, a hybrid multi-reference ANC (HMRANC) is proposed in this paper. However, the practical challenge associated with both HANC and the proposed HMRANC controller is the increase in computational burden.

The computational complexity of adaptive filters can be reduced by using frequency-domain filtering techniques based on decomposing, processing, and reconstructing the signals using filter banks such as subband adaptive filtering (SAF) and block adaptive filtering (BAF) techniques [20, 21, 22]. The major drawback of conventional SAF is that a delay is introduced into the signal path by virtue of the bandpass filters used to derive the subband signals [23]. For active noise control, the primary path delay should be larger than the total secondary path delay (which comprises of adaptive filter and secondary path) to maintain the causality condition. Therefore, to avoid introducing an additional delay into the secondary path, a delayless SAF technique was proposed by Morgan et al. [23], in which the adaptive weights are computed in subbands and then transformed to an equivalent wideband filter [22, 24, 25, 26]. Several studies have demonstrated that the performance of ANC headsets relies on the timely detection of the reference signal and the delays in the secondary path [16, 8, 9]. Therefore, to reduce the computational burden without violating the causality constraints while utilizing reference signals from both reference microphones mounted on both the left and right ear cups, a delayless subband implementation of the proposed HMRANC system is also presented in this paper.

The paper is organised as follows. Section 2 introduces the proposed

HMRANC structure for the headphone application along with a discussion on the computational requirements for HMRANC. To reduce the computational demand of HMRANC, a delayless subband implementation of HMRANC is presented in Section 3. A comparative study on the computational requirements of the HMRANC and delayless subband HMRANC systems is discussed in Section 3.1. The performance of the proposed ANC headphone strategy is investigated through experimental testing and these results are presented in Section 4 along with the corresponding results for existing ANC systems for different ambient sound fields. Finally, concluding remarks are presented in Section 5.

2. Proposed HMRANC

As noted in the introduction, HANC has been shown to offer improved performance over feedforward or feedback ANC systems operating in isolation in headphones [6]. It has also been highlighted how a multi-reference ANC strategy can improve the performance of ANC headphones with respect to controlling sources of noise originating from various directions [16]. Therefore, this section will describe a system that combines these two approaches to realise a Hybrid Multi-reference ANC (HMRANC) system. The basic system will first be described in Section 2.1 and the computational complexity of this system will be described in Section 2.2.

2.1. Hybrid Multi-Reference Active Noise Control System

The proposed hybrid multi-reference ANC system (HMRANC) for the headphone application is shown in Figure 1 for the left ear controller. In this figure, the light gray region corresponds to the multi-reference feedforward

control component, whilst the dark gray region encompasses the feedback component. In the HMRANC system the control signal, $u_L(n)$, for the left ear is given by the summation of the control signals generated by the multi-reference feedforward controller and feedback ANC controller, which can be written as

$$u_L(n) = u_{LL}(n) + u_{RL}(n) + u_{FBL}(n), \quad (1)$$

where $u_{LL}(n)$, $u_{LR}(n)$ are the control signals associated with the multi-reference feedforward controller and $u_{FBL}(n)$ is the control signal associated with the feedback controller. In the above expression, $u_{LL}(n) = \mathbf{w}_{LL}^T(n)\mathbf{x}_L(n)$, where $\mathbf{x}_L(n) = [x_L(n), x_L(n-1), \dots, x_L(n-N_1+1)]^T$ is the tap-delayed vector of the signal sensed by the left reference microphone on the left ear-cup and $\mathbf{w}_{LL}(n) \in \mathbb{R}^{N_1 \times 1}$ corresponds to the control filter whose input is from the left reference microphone and is used to control the noise at the left ear error microphone. Similarly, $u_{LR}(n) = \mathbf{w}_{LR}^T(n)\mathbf{x}_R(n)$, where $\mathbf{x}_R(n) = [x_R(n), x_R(n-1), \dots, x_R(n-N_2+1)]^T$ is the tap-delayed vector of the signal sensed by the reference microphone on the right ear-cup of the headphone, and $\mathbf{w}_{LR}(n) \in \mathbb{R}^{N_2 \times 1}$ corresponds to the control filter whose input is from the right reference microphone and is used to control the noise at the left ear of the headphone system. Finally, $u_{FBL}(n) = \mathbf{x}_{FBL}^T(n)\mathbf{w}_{FBL}(n)$ with $\mathbf{x}_{FBL}(n) = [x_{FBL}(n), x_{FBL}(n-1), \dots, x_{FBL}(n-N_3+1)]^T$ is the tap-delayed vector of the estimate of the disturbance signal at the left ear error microphone inside the ear cup of the headphone system and $\mathbf{w}_{FBL} \in \mathbb{R}^{N_3 \times 1}$ is the weight vector for the feedback controller for the left ear of the headphone.

The weights of both the feedforward and feedback control filters are up-

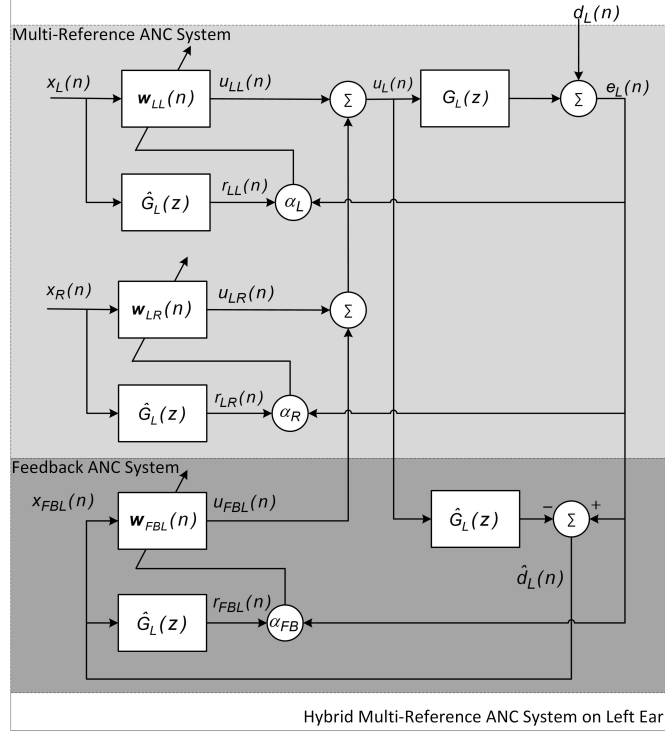


Figure 1: Block diagram of the HMRANC system for the left ear of the headphones; the equivalent block diagram for the right ear controller can be obtained by interchanging the L and R subscripts.

dated using the filtered-x LMS algorithm [27, 3], and are given as

$$\begin{aligned}
 \mathbf{w}_{LL}(n+1) &= \mathbf{w}_{LL}(n) - \alpha_{LL} \mathbf{r}_{LL}(n) e_L(n) \\
 \mathbf{w}_{LR}(n+1) &= \mathbf{w}_{LR}(n) - \alpha_{LR} \mathbf{r}_{LR}(n) e_L(n) \\
 \mathbf{w}_{FBL}(n+1) &= \mathbf{w}_{FBL}(n) - \alpha_{FBL} \mathbf{r}_{FBL}(n) e_L(n)
 \end{aligned} \tag{2}$$

where α_{LL} , α_{LR} and α_{FBL} are the convergence gains, $\mathbf{r}_{LL}(n) \in \mathbb{R}^{N_1 \times 1}$, $\mathbf{r}_{LR}(n) \in \mathbb{R}^{N_2 \times 1}$ and $\mathbf{r}_{FBL}(n) \in \mathbb{R}^{N_3 \times 1}$ are the filtered versions of the reference signals, $x_L(n)$, $x_R(n)$ and $x_{FBL}(n)$, obtained by filtering the reference

signal through a model of the plant response between the left loudspeaker and the left error microphone, $\hat{G}_L(z)$. To simplify the analysis it has been assumed that all three of the control filters have the same length, such that $N_1 = N_2 = N_3 = N$, although it is possible to modify the lengths of the control filters depending on the requirements. The error signal at the left ear can be expressed as

$$e_L(n) = d_L(n) + \mathbf{g}_L^T \mathbf{u}_L(n), \quad (3)$$

where $d_L(n)$ is the disturbance signal at the left error microphone, \mathbf{g}_L is the vector of filter coefficients representing the impulse response of the plant $\hat{G}_L(z)$, and the left side control loudspeaker is driven by the control signal vector $\mathbf{u}_L(n)$. The three update equations defined in equation (2) can be written in a more compact form as

$$\mathbf{w}_L(n+1) = \mathbf{w}_L(n) - \mathbf{r}_L^T(n)e_L(n), \quad (4)$$

where $\mathbf{w}_L(n)$ is the concatenation of weight vectors from (2) given as $\mathbf{w}_L(n) = [\mathbf{w}_{LL}^T(n), \mathbf{w}_{LR}^T(n), \mathbf{w}_{FBL}^T(n)]^T$ and $\mathbf{r}_L(n)$ is a vector of size $3N \times 1$ given as

$$\mathbf{r}_L(n) = [\alpha_{LL}\mathbf{r}_{LL}^T(n), \alpha_{LR}\mathbf{r}_{LR}^T(n), \alpha_{FBL}\mathbf{r}_{FBL}^T(n)]^T. \quad (5)$$

2.2. HMRANC Computational Complexity

The computational demand of the HMRANC implementation shown in Figure 1 is mainly due to updating the control filter weights, generation of the filtered reference signal and the control signal generation. To update the weights of the controller $3N + 3$ multiplications are required. However, for

control signal and filtered reference signal generation $3N$ and $3L$ multiplications are required, where L is the length of the plant model filter, $\hat{g}_L(n)$. In addition, to generate the internal reference signal for the feedback controller, L multiplications are also needed. Thus, the total number of multiplications required by HMRANC is $6N + 4L + 3$ which is approximately three times more computationally demanding compared to a conventional single reference feedforward ANC (FFANC) system which requires $2N + L + 1$ multiplications. The increase in computational demand is due to the additional reference signal provided by the reference microphone mounted on the opposite ear cup and due to the internal reference signal generated by the feedback controller. However, the proposed HMRANC strategy offers improved noise attenuation capability compared to the traditional FFANC and HANC strategies, as will be presented in Section 4. Therefore, in-order to reduce the computational load, a delayless subband implementation of the HMRANC strategy is presented in the following section.

3. Delayless Subband Hybrid Multi-Reference Active Noise Control System

The delayless subband implementation of the HMRANC system decomposes the model of the plant response, $\hat{G}_L(z)$, and the control filter coefficient update process into a number of subbands, as shown in Figure 3. In this block diagram it can be seen that all three reference signals and the error signal are decomposed into corresponding subband components by filtering through an analysis filter-bank, $\mathbf{h}(z)$. There are a number ways of implementing the analysis filter bank and all of these methods provide a trade-off between

spectral leakage, delay and computational complexity [28, 29]. It has been reported by Milani *et al* [24], that by using a Uniform Discrete Fourier Transform Modulated (UDFTM) filter-bank, minimal delay is introduced into the system loop in comparison to other available analysis filter bank design techniques. Since the performance of an ANC system is degraded by the delay associated with the system, the UDFTM filter-bank has been employed as the analysis filter bank having the transfer function $\mathbf{h}(z)$ given as

$$\mathbf{h}(z) = [H_0(z) \quad H_1(z) \quad \cdots \quad H_{M-1}(z)] \quad (6)$$

where $H_m(z) = H_0(ze^{-j2\pi m/M})$ and $H_0(z) = 1 + z^{-1} + z^{-2} + \cdots + z^{-M+1}$ is a M -coefficient prototype low-pass filter. The magnitude response of $H_0(e^{j\Omega})$ for $M = 16, 32$, and 64 is shown in Figure 2. As shown by the responses in Figure 2, the first zero crossing of $H_0(e^{j\Omega})$ occurs at $2\pi/M$ and this gives a bandwidth of $2\pi/M$. The central frequency of the bandpass filters $H_m(z)$ in the filter bank is located at $\Omega_m = 2\pi m/M$. The UDFTM filter-bank can be expressed in terms of the M^{th} order discrete Fourier transform (DFT) matrix as

$$\mathbf{h}(z) = \frac{1}{M} F^* \left[1, z^{-1}, \dots, z^{-M+1} \right]^T \quad (7)$$

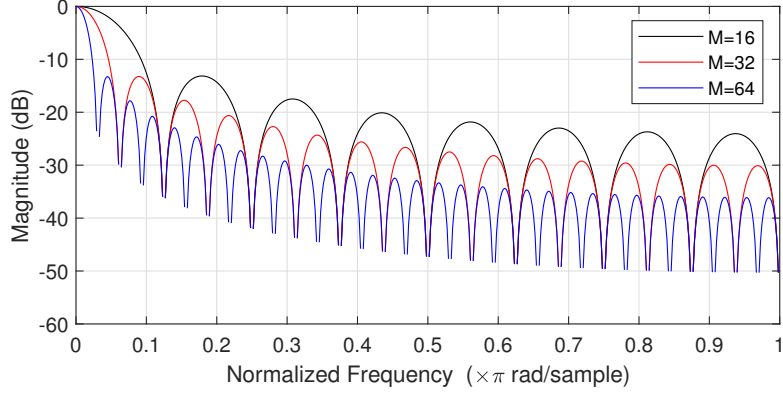


Figure 2: Magnitude frequency response of $H_0(e^{j\Omega})$ for $M = 16, 32,$ and 64

where F is the DFT matrix and $*$ is the complex conjugate operator. The implementation of the UDFTM filter bank can be realized by using a tapped delay line of length M followed by an inverse FFT block [26]. The output of the analysis filter bank designed using UDFTM is complex in nature, thus the weights in each subband are updated using the complex FxLMS algorithm, given for the m^{th} band as

$$\mathbf{w}_{L,m}(n+1) = \mathbf{w}_{L,m}(n) - \mathbf{r}_{L,m}^T(n)e_{L,m}(n), \quad (8)$$

where, $\mathbf{w}_{L,m}$ is the weight vector of size $3N_{SAF} \times 1$ for the m^{th} subband, and $N_{SAF} = \frac{4N}{M}$ [24]. The reference vector $\mathbf{r}_{L,m}$ is given as

$$\mathbf{r}_{L,m}^T(n) = [\alpha_{LL,m}\mathbf{r}_{LL,m}^T(n), \alpha_{LR,m}\mathbf{r}_{LR,m}^T(n), \alpha_{FBL,m}\mathbf{r}_{FBL,m}^T(n)]^T, \quad (9)$$

where $\mathbf{r}_{LL,m}^T(n)$, $\mathbf{r}_{LR,m}^T(n)$, and $\mathbf{r}_{FBL,m}^T(n)$ are the filtered reference signals, $e_{L,m}(n)$ is the error signal and $\alpha_{LL,m}$, $\alpha_{LR,m}$, and $\alpha_{FBL,m}$ are the convergence gains for the m^{th} subband. Furthermore, it has also been suggested that by using a higher number of subbands and employing the UDFTM filter-bank

a significant computational saving can be achieved [26]. Another point to be highlighted here is that the subband decomposition of the reference signals, error signal and the plant model makes it possible to implement the filtered reference signal generation and weight update stage at a reduced sampling rate, F_s/D , where D is the decimation factor [23]. An appropriate choice of decimation factor is required to avoid side-lobes in the analysis filter bank, which result in aliasing and degrade the noise cancellation efficiency of the ANC system. To limit the aliasing effect Milani *et al.* [24] have employed a decimation factor of $D = M/4$, which makes it possible to use a higher number of subbands as compared to the method proposed by Morgan and Thi [23], and this further reduces the overall computational burden.

To reconstruct the full band filter, $\mathbf{w}_L(z)$, from the M subband filter weights, $\mathbf{w}_{L,m}$, a weight stacking process is needed. In the weight stacking process, each of the subband filter weights corresponding to each reference signal are transformed to the frequency domain using a $2N_{SAF}$ point FFT. These frequency domain weights are then stacked together to form the broadband filter response in the frequency domain [22]. Finally, the frequency domain representation of the broadband filter is transformed back to the time domain. In this weight stacking method, the number of filter weights required in each subband should be greater than or equal to $4N/M$ [22].

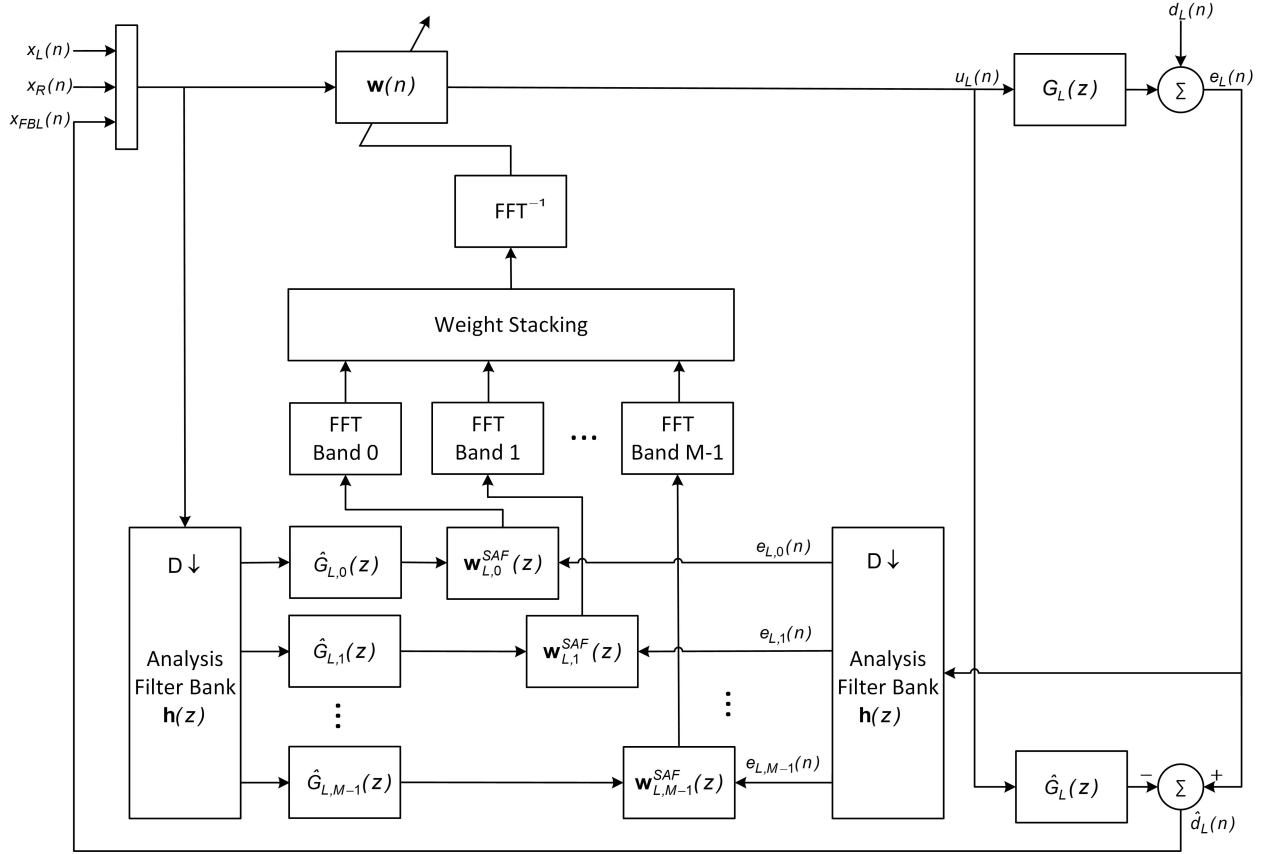


Figure 3: Block diagram of the delayless subband HMRANC system for the left ear of the headphones; the equivalent block diagram for the right ear controller can be obtained by interchanging the L and R subscripts.

3.1. Delayless Subband HMRANC Computational Complexity

In this section the computational complexity of the proposed delayless subband HMRANC system is calculated in-terms of the number of multiplications required per iteration. The processing of the delayless subband HMRANC system can be divided into the following subunits:

1. Subband Filtering

The analysis filter bank for subband filtering can be implemented using an M -point IFFT [24]. Thus, in order to filter 3 reference signals and 1 error signal, $4M\log_2 M$ multiplications are required per sample at the full sample rate, F_s . However, by employing the Noble identity, the M -point IFFT can be performed at a decimated sample rate of F_s/D [26, 30], this leads to a computational demand in terms of multiplications of

$$C_1 = 4 \frac{M \log_2 M}{D}. \quad (10)$$

2. Filtered reference signal generation

The filtered reference signals for the delayless subband implementation shown in Figure 3 are obtained by using subband plant models instead of fullband plant models as required with a conventional FxLMS implementation [30]. The number of coefficients in each subband plant model filter is $L_{SAF} = \frac{4L}{M}$ [22, 26]. The number of real multiplications required per sample is thus given as

$$C_2 = 3 \left[3L_{SAF} \left(\frac{M/2 + 1}{D} \right) \right] = 3 \left[\frac{12L}{M} \left(\frac{M/2 + 1}{D} \right) \right], \quad (11)$$

where D is the decimation factor, the 3 outside the square brackets corresponds to the complex filtering since the reference signals are complex in nature as discussed in the previous section, the 3 inside the square brackets corresponds to the 2 reference signals from each reference microphone and the internally generated reference signal required by the feedback ANC system. To implement the subband version of the plant model filtering stage,

$M/2 + 1$ subbands have been employed [24, 28, 23].

3. Subband adaptive weight update

The complex LMS update in (8) and (9) requires $3N_{SAF}$ complex and 6 real multiplications to generate $\mathbf{r}_{L,m}(n)$. Each complex multiplication can be accomplished using a minimum of 3 real multiplications, which leads to a total of $9N_{SAF} + 6$ real multiplications, where $N_{SAF} = \frac{4N}{M}$. The weights of the $M/2 + 1$ subbands needs to be updated every D samples, therefore, the weight update stage for the delayless subband structure shown in Figure 3 requires

$$C_3 = (9N_{SAF} + 6) \left(\frac{M/2 + 1}{D} \right) = \left(36 \frac{N}{M} + 6 \right) \left(\frac{M/2 + 1}{D} \right) \quad (12)$$

real multiplications.

4. Weight stacking and time domain transformation

To transfer the subband weights to the fullband weights requires three $2N_{SAF}$ -point complex FFTs for the $(M/2 + 1)$ subbands and a $2N$ -point inverse FFT for each of the three reference signals, thus the total number of real multiplications required per D samples is given by

$$\begin{aligned} C_4 &= \frac{3[(M/2 + 1)4N_{SAF}\log_2 2N_{SAF} + 2N\log_2 2N]}{D} \\ &= \frac{3[(M/2 + 1)\frac{16N}{M}\log_2 \frac{32N}{M} + 2N\log_2 2N]}{D}. \end{aligned} \quad (13)$$

5. Control signal generation

The final element of the subband implementation is the generation of the control signal, which as shown in Figure 3, has been performed in the time domain and it requires

$$C_5 = 3N \quad (14)$$

real multiplications. The 3 once again corresponds to the two reference signals, one from each reference microphone, and the internal reference signal generated by the feedback controller.

3.2. Comparison of computational complexity

Table 1 summarizes the computational complexity of the proposed delayless subband HMRANC, along with the HMRANC system, MRANC system, single reference ANC system, i.e., the conventional FFANC system, and the HANC system in terms of the number of real multiplications per sample for one ear of the system. As suggested in [16], it is worth noting that the length of acoustic path between the left reference and left error microphone is smaller compared to the acoustic path between the right reference and left error microphones, thus it could be possible to choose $N_2, N_3 < N_1$ without degrading the attenuation performance of the HMRANC system, which leads to a lower computational load. **The number of real multiplications required by FFANC, MRANC, HANC, HMRANC, and the delayless subband HMRANC algorithms, with the assumption that $N_1 = N_2 = N_3 = N$ with $N = 256$, $L = 256$, and $D = M/4$ is shown in Figure 4.**

From Figure 4, it can be seen that for a lower number of subbands

Table 1: Computational complexity comparison between the feedforward ANC (FFANC), multi-reference feedforward ANC (MRANC), hybrid ANC (HANC), multi-reference hybrid ANC (HMRANC), and delayless subband HMRANC, based on the number of real multiplications per sample.

	FFANC	MRANC	HANC	HMRANC	Delayless Subband HMRANC
Subband filtering	none	none	none	none	$4 \frac{M \log_2 M}{D}$
Filtered reference signal generation	L	$2L$	$2L$	$3L$	$3 \left[3L_{SAF} \left(\frac{M/2+1}{D} \right) \right]$
Weight update	$N + 1$	$2N + 1$	$2N + 1$	$3N + 1$	$(15N_{SAF} + 1) \left(\frac{M/2+1}{D} \right)$
Weight stacking and time domain transformation	none	none	none	none	$\frac{3[(M/2+1)4N_{SAF} \log_2 2N_{SAF} + 2N \log_2 2N]}{D}$
Internal reference signal generation	none	none	L	L	L
Control signal generation	N	$2N$	$2N$	$3N$	$3N$
Total	$2N + L + 1$	$4N + 2L + 1$	$4N + 3L + 1$	$6N + 4L + 1$	$3N + \frac{4M \log_2 M + 9L_{SAF}(M/2+1)}{D} + \frac{(M/2+1)[(15N_{SAF}+1) + (12N_{SAF} \log_2(2N_{SAF}))]}{D} + \frac{[6N \log_2(2N)]}{D} + L$

($M \leq 64$), the computational complexity of delayless subband HMRANC is higher than HMRANC. However, for $M = 256$ the number of multiplications required by delayless subband HMRANC is 40% less than HMRANC and 10% lower than HANC, and almost equal to that required by MRANC. It can also be seen from Figure 4 that the computational burden of the delayless subband HMRANC is around half of that required by HRMANC for $M = 512$.

Figure 5 demonstrates the variation in the number of real multiplications as a function of input memory size, N , while keeping $L = 256$ and $M = 256$. From Figure 5 it can be seen that for lower values of N the computational load of the proposed delayless subband HMRANC is lower than MRANC, HANC and HMRANC. Moreover, for $N = 256$ the computational burden of the delayless subband HMRANC is the same as the MRANC algorithm, however, as N increases beyond 256, the number of multiplications required by the

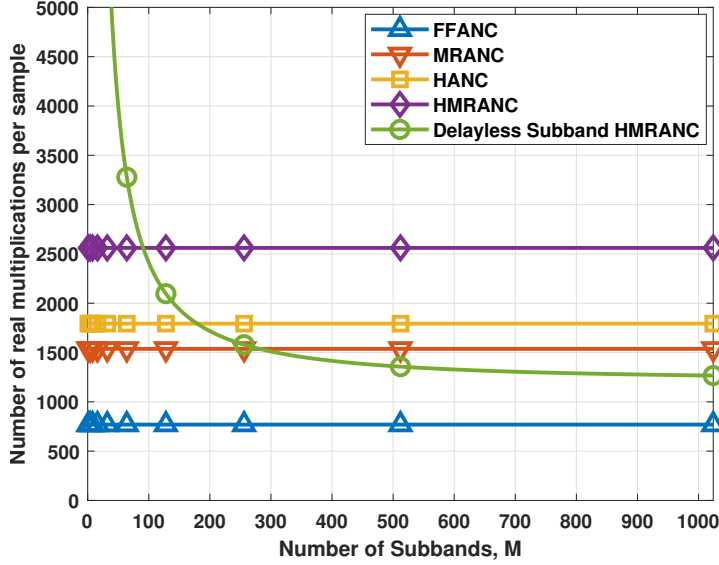


Figure 4: Number of real multiplications required per sample for FFANC, MRANC, HANC, HMRANC and delayless subband HMRANC systems for $D = M/4$, $N = 256$, and $L = 256$.

delayless subband HMRANC starts increasing approximately 2 times faster with N compared to HANC.

The number of real multiplications required per sample for FFANC, HANC, HMRANC, and delayless subband HMRANC are plotted in Figure 6 as a function of secondary path length, L , while keeping $N = 256$ and $M = 256$. It can be seen from Figure 6 that the computational complexity of delayless subband HMRANC is higher than FFANC, HANC, and MRANC for $L \leq 128$. However, as L increase beyond 128 the number of multiplications required by the delayless subband HMRANC starts decreasing and for $L = 256$ the computational burden of delayless subband HMRANC becomes equal to MRANC.

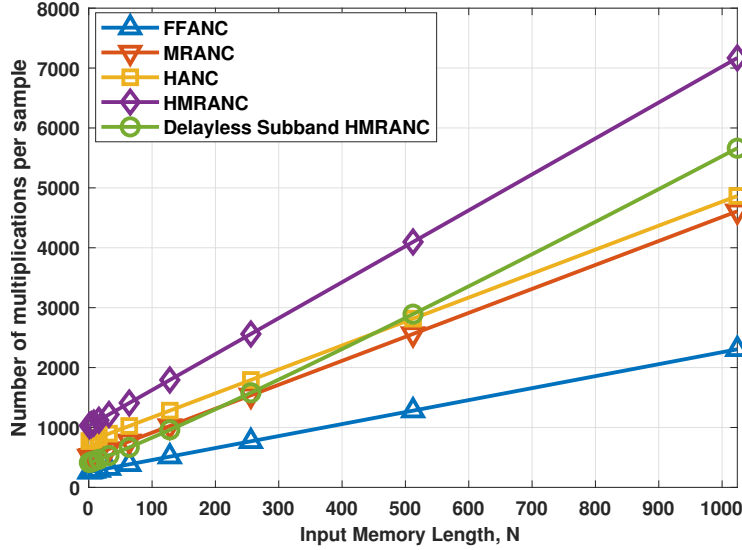


Figure 5: Number of real multiplications required per sample with respect to input memory size, N for FFANC, MRANC, HANC, HMRANC and delayless subband HMRANC systems for $D = M/4$, $M = 256$, and $L = 256$.

4. Experimental Study

The experimental set-up used to validate the performance of the proposed HMRANC system is shown in Figure 7(a). All 5 of the control algorithms have been implemented on a dSPACE MicroLabBox at a sampling rate of $Fs = 16\text{kHz}$ and primary disturbance is a first order auto-regressive AR(1) process obtained by filtering a white Gaussian noise via the first order system $H(z) = \frac{1}{1-0.9z^{-1}}$. The impulse responses corresponding to the left and right ear plants are shown in Figure 8. The plant responses for the left and right ear are modelled using FIR filters of $L = 256$, whilst each control filter is designed using an $N = 256$ FIR filter. The performance of ANC headphones is known to be dependent on the direction of the incident sound field [16], therefore,

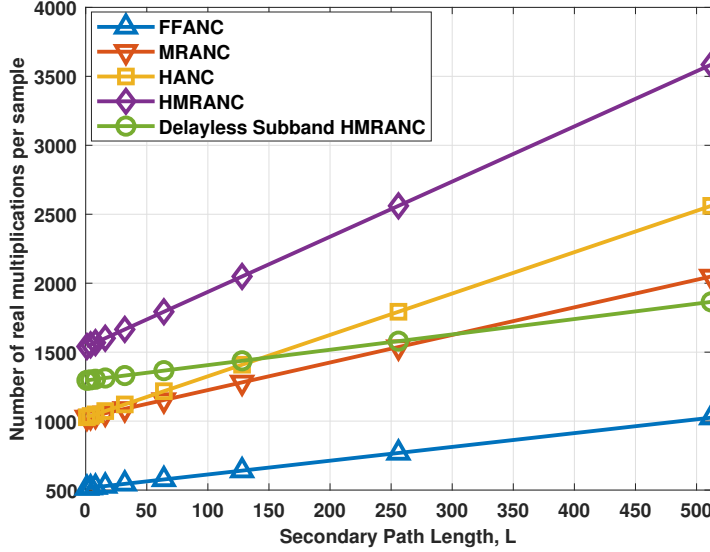


Figure 6: Number of real multiplications required per sample with respect to secondary path length, L for FFANC, MRANC, HANC, HMRANC and delayless subband HMRANC systems for $D = M/4$, $N = 256$, and $M = 256$.

three different cases have been considered here: Firstly, when the primary noise source is in front of the user; secondly, when the primary noise source is at the right of the user, and finally, when the primary noise is generated by multiple loudspeakers surrounding the user. The convergence gain for all of the algorithms is chosen in order to achieve the maximum convergence speed, and the convergence gain of the delayless subband HMRANC system is set as discussed in [26]. Normalised Mean Square Error (NMSE) is used to evaluate the noise attenuation achieved by each of the ANC systems, given as

$$\text{NMSE}(n) = 10 \log_{10} \left[\frac{d^2(n)}{e^2(n)} \right], \quad (15)$$

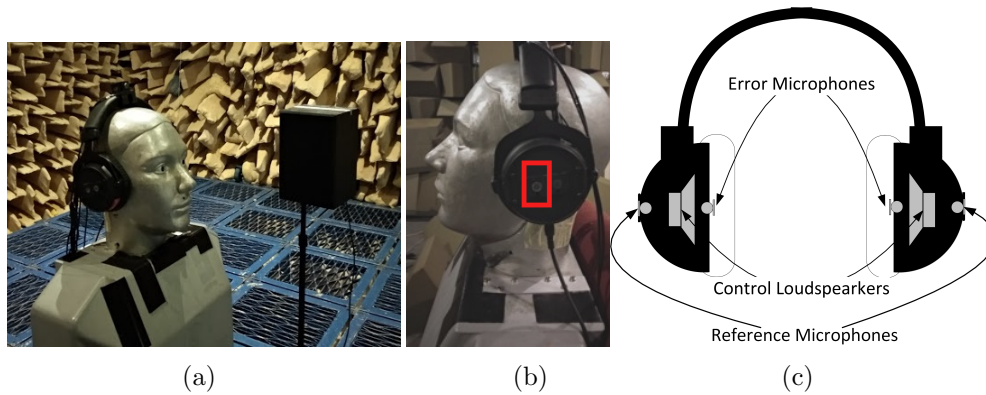


Figure 7: (a) Experimental setup used with the primary noise source located on the axis line of both ears. (b) Photo of the prototype headphone; note, reference microphone is inside the red box on ear cup (left ear), in a similar way another reference microphone is placed on the right ear cup. (c) Schematic of ANC headphone configuration showing the locations of the error microphone inside each ear cup, the reference microphones located on the outside of each ear cup and the control loudspeakers.

The convergence speed is measured in terms of the time taken by the headphone control strategies to reach a specified NMSE level of χ dB, and this is labelled as τ_χ .

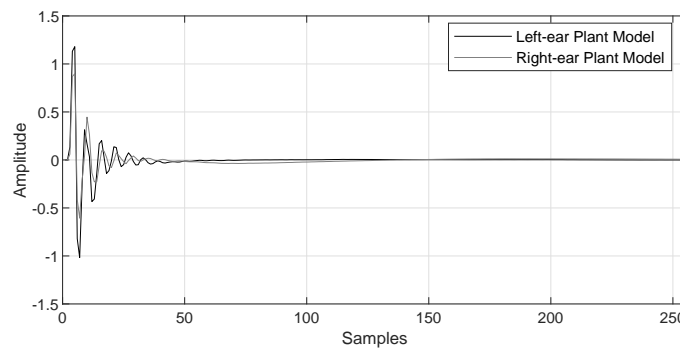


Figure 8: Impulse response of the left and right ear plant models.

4.1. Case I: Primary noise source positioned in front of the user

In the first case, the primary noise source is placed in front of the user. Before investigating the noise attenuation capability of the underlying ANC algorithms, an analysis is conducted to determine the effect of the number of subbands on the rate of convergence and the steady-state performance of delayless subband HMRANC.

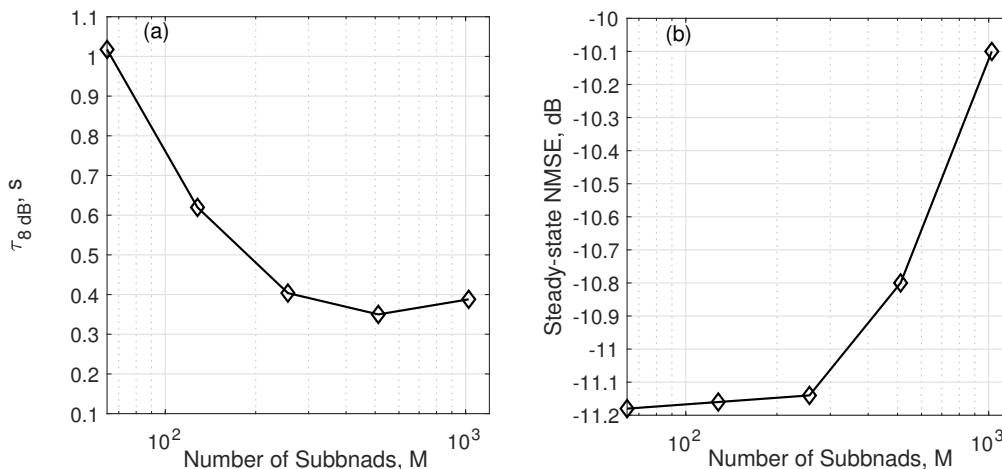


Figure 9: (a) The time taken by the delayless subband HMRANC to achieve an noise attenuation of 8 dB at the left-ear error microphone for different numbers of subbands, $64 \leq M \leq 1024$. (b) Steady-state NMSE value achieved by the delayless subband HMRANC at the left-ear error microphone for different numbers of subbands, $64 \leq M \leq 1024$.

Figure 9(a) shows the time taken by the delayless subband HMRANC to achieve a noise attenuation of 8 dB at the left-ear error microphone for different numbers of subbands. Figure 9(b) shows the steady-state NMSE value achieved by the delayless subband HMRANC obtained by averaging the last 1000 samples. The minimum number of subbands is set at 64 since

for smaller number of subbands ($M \leq 64$) the computational complexity of the delayless subband HMRANC is very high compared to HMRANC as shown in Figure 4. From Figures 9(a) and 9(b), it can be seen that with an increase in the number of subbands, M , the convergence rate of the delayless subband HMRANC increases, while the steady-state noise mitigation performance slightly deteriorates as M increases. Therefore, to reach a trade-off between convergence rate, steady-state noise attenuation, and computational complexity for the delayless subband HMRANC, the number of subbands is set to $M = 256$ in all the following experiments.

The convergence characteristics and spectra of the microphone signals before and after control achieved by the five algorithms are shown in Figures 10 and 11, and Table 2 summarise the broadband levels of attenuation. As seen from Figure 10 and Table 2, both the FFANC and MRANC achieve a broadband attenuation of 10.9 dB and 11.7 dB for the left and right ears respectively. It is expected that these two strategies would perform similarly because, with this primary source configuration, there is no time-advance provided by the additional reference signals, as discussed in [16]. The noise attenuation achieved by HANC, HMRANC, and delayless subband HMRANC is 11.1 dB and 11.9 dB at the left and right ears. The slight improvement in these cases is due to the feedback ANC controller acting simultaneously with the feedforward control mechanism. The improvement achieved by the hybrid controller can be better visualised from the spectrum of the error signal before and after control as shown in Figure 11; these spectra are computed after the convergence of the algorithms. From Figure 11, an improvement of 2-3 dB can be seen in the frequency bands between 125 Hz to 500 Hz

for the three hybrid controllers: HANC, HMRANC and delayless subband HMRANC ($M = 256$).

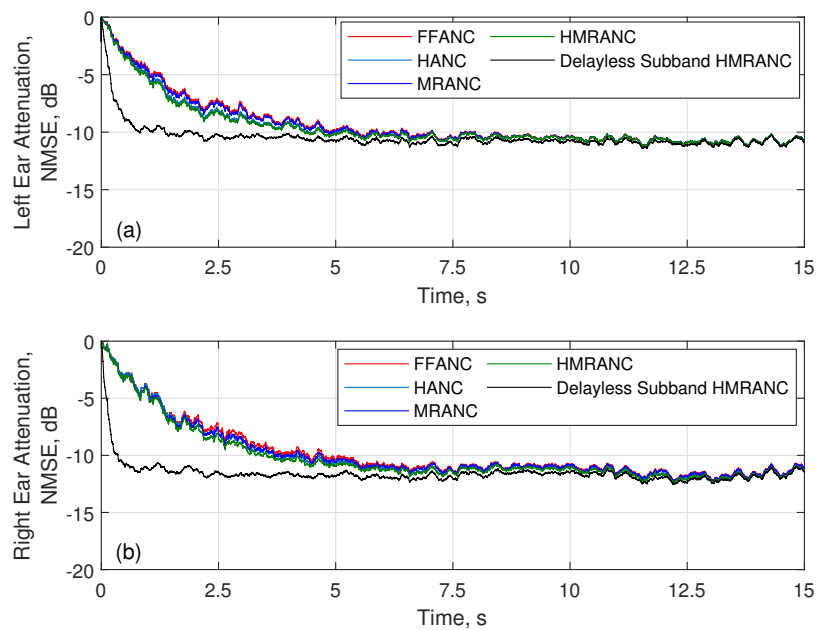


Figure 10: Convergence characteristics of FFANC, HANC, MRANC, HMRANC, and delayless subband HMRANC for left (a) and right (b) ear.

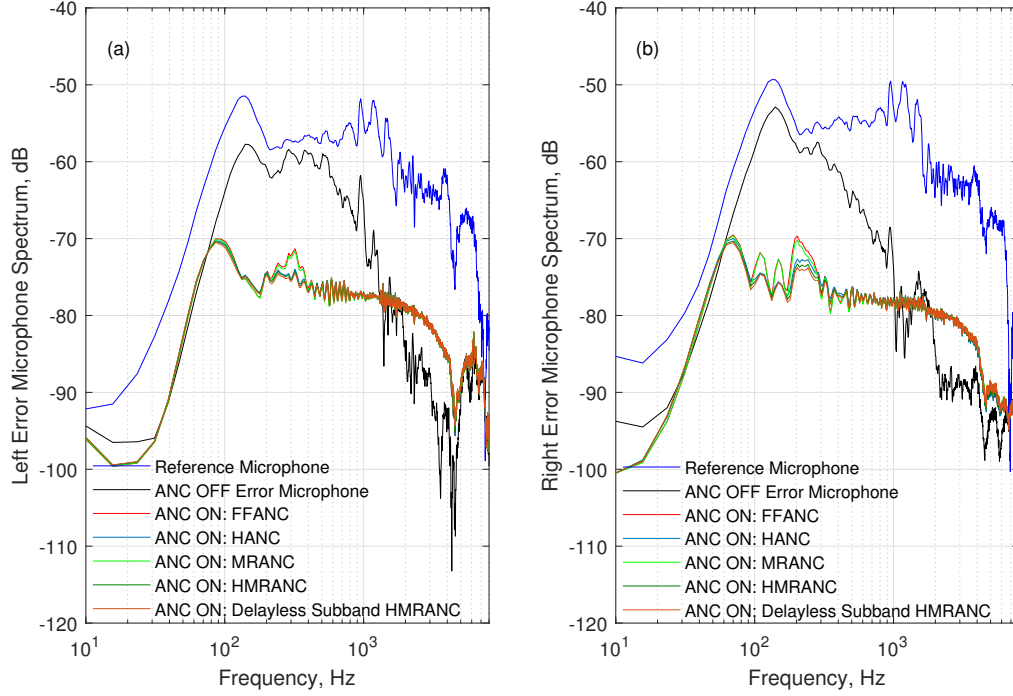


Figure 11: Active attenuation achieved on the left and right error microphone by FFANC, MRANC, HANC, HMRANC and Delayless Subband HMRANC strategy for noise incident from the front of user.

Table 2: Steady-state NMSE(dB) achieved by FFANC, HANC, MRANC, HMRANC, delayless subband HMRANC at the left and right ear.

	Case-I		Case-II		Case-III	
	Left ear	Right ear	Left ear	Right ear	Left ear	Right ear
FFANC	-10.9	-11.7	-6.3	-21.9	-18.2	-18.8
HANC	-11.1	-11.9	-6.5	-26.9	-20.4	-21.8
MRANC	-10.9	-11.9	-23.7	-24.5	-22.8	-24.8
HMRANC	-11.1	-11.9	-25.0	-27.5	-25.1	-26.6
Delayless Subband HMRANC	-11.1	-11.9	-25.0	-27.6	-25.1	-26.6

It is evident from Figure 10 and 11 that the delayless subband HMRANC system achieves similar noise attenuation to HMRANC with a faster convergence rate. ~~Moreover, with the current set-up,~~ the delayless subband HMRANC ($M=256$) requires 1578 multiplications which is approximately 40% less computationally demanding than HMRANC which needs 2561 multiplications and 10% less demanding than HANC algorithms which requires 1793 multiplications, respectively. Similar performance characteristics are shown by the HMRANC and delayless subband HMRANC algorithm when the primary noise source is placed at the rear of the user due to the similarity of the setup.

4.2. Case II: Primary noise source positioned to the right of the user

To demonstrate the advantage of the multi-reference strategies, the performance is evaluated when the direction of incidence of the primary noise source is located to the right of the user, that is, when the primary noise source is along the line passing through both ears. In this scenario the primary disturbance reaches one ear before the other and this time advance is used by the multi-reference ANC strategy to achieve increased noise attenuation [16]. The convergence characteristics of all five algorithms are shown in Figure 12. The improvement in the noise attenuation performance achieved by the MRANC, HMRANC and delayless subband HMRANC is evident from Figure 12. Figure 13 shows the spectrum measured before and after control for each of the five algorithms at the left and right error microphones. The steady state NMSE achieved for each of the algorithms is summarised in Table 2. From these results it is clear that the attenuation at the right ear, for both the conventional HANC and HMRANC strategy is almost the same

since there is no time advanced information available for the right ear, with the primary disturbance located to the right-side of the user. The improved convergence rate of delayless subband HMRANC is also evident from Figure 12.

It can be seen from the presented results for this configuration that the noise attenuation achieved by HANC, HMRANC and delayless subband HMRANC is 5–10 dB higher than achieved by the FFANC and MRANC algorithms, especially in the frequency band from 125 Hz to 500 Hz due to the feedback controller incorporated in HANC and HMRANC, as can be seen from Figure 13. The proposed delayless subband HMRANC ($M = 256$) requires 1578 multiplications which is same as required by MRANC and 50% more computationally expensive than the conventional FFANC system which requires 769 multiplications as demonstrated from the results presented in Figure 4 and Table 1, whilst showing an improvement of 18 dB and 6 dB in noise attenuation for the left and right ears respectively. Similar improvements are also shown for HMRANC and the delayless subband HMRANC system on the right ear, when the primary disturbance source is instead placed on the left of the user. 

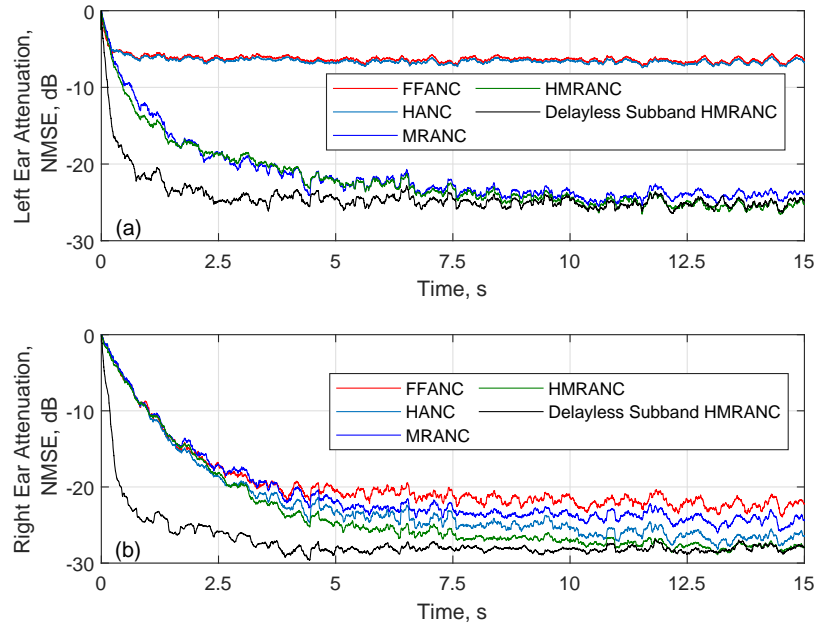


Figure 12: Convergence characteristics of FFANC, HANC, MRANC, HMRANC, and delayless subband HMRANC ($M = 256$) for left (a) and right (b) ear.

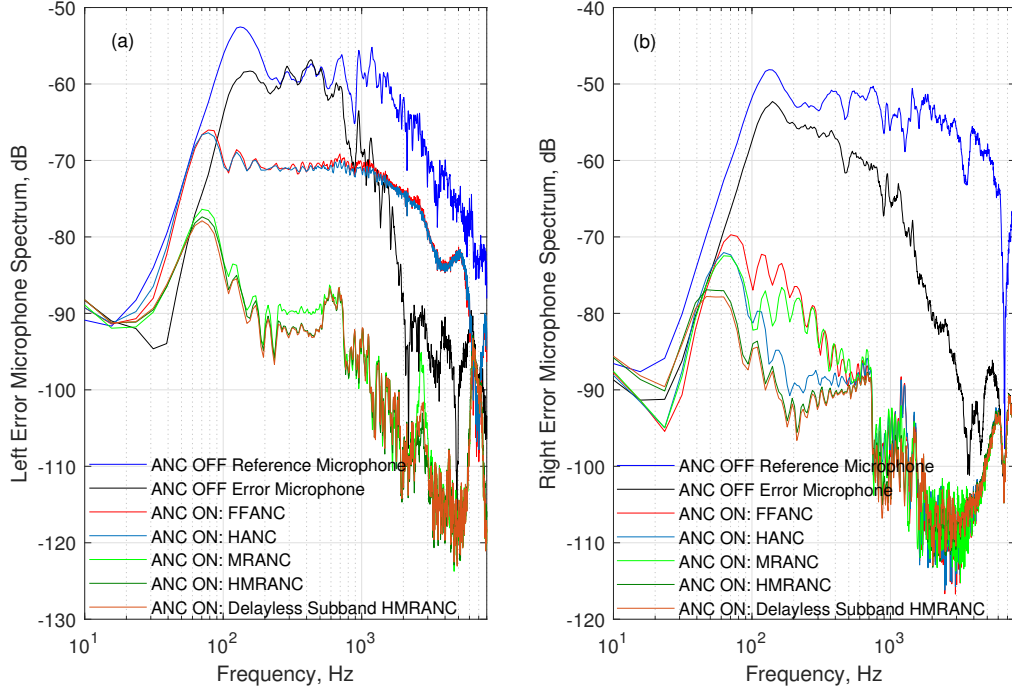


Figure 13: Active attenuation achieved on the left and right error microphone by FFANC, MRANC, HANC, HMRANC and delayless subband HMRANC strategy for noise incident from right side of user.

4.3. Case III: Multiple primary noise sources positioned around the user

In the third case, the performance of each of the ANC headphone strategies is compared in a more realistic scenarios. An experiment is conducted in which the uncorrelated primary noise is incident from all the 12 directions around the dummy head as shown in Figure 14. The convergence characteristics for the five control strategies are shown in Figure 15. The improved noise attenuation performance achieved by the HMRANC and delayless subband HMRANC strategies is evident from Figure 15. The spectra of the signals

measured at the left and right error microphones for all five algorithms are shown in Figure 16. The steady state NMSE achieved by FFANC, HANC, MRANC, HMRANC, and delayless subband HMRANC for the left and right ears is shown in Table 2, along with the results for the other two cases. Under this more practical scenario, it can be seen that HMRANC and delayless subband HMRANC achieve 5 dB more noise attenuation at both the left and right ears compared to the HANC headphone system. **The improved convergence rate of delayless subband HMRANC is also evident from Figure 15 and this is all achieved at a computational load of 1578 multiplications which is 10% lower than the HANC headphone systems which requires 1793 multiplications.**

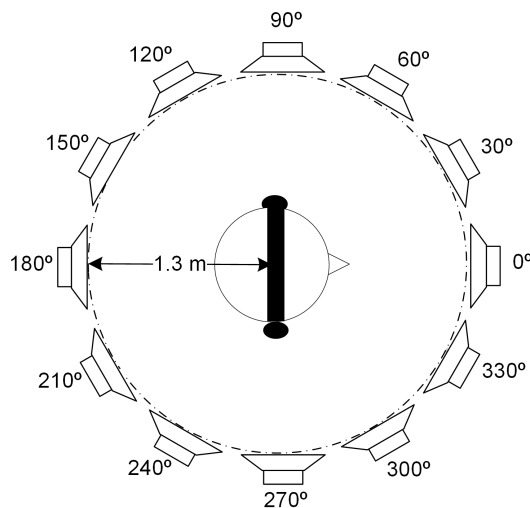


Figure 14: **Schematic of the experimental test configuration with primary sources positioned at angular increments of 30 degrees at a radial distance of 1.3 m around the dummy head.**

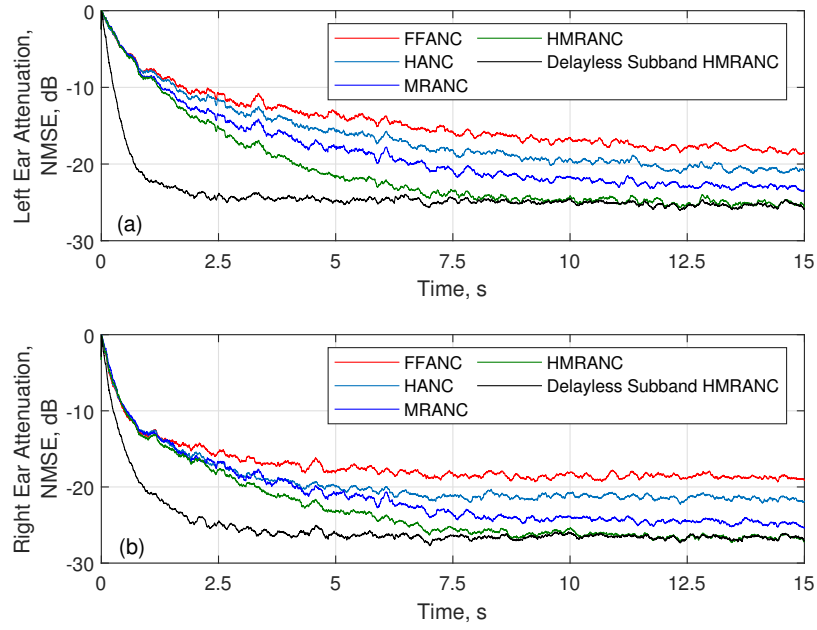


Figure 15: Convergence characteristics of FFANC, HANC, MRANC, HMRANC, and delayless subband HMRANC for left (a) and right (b) ear.

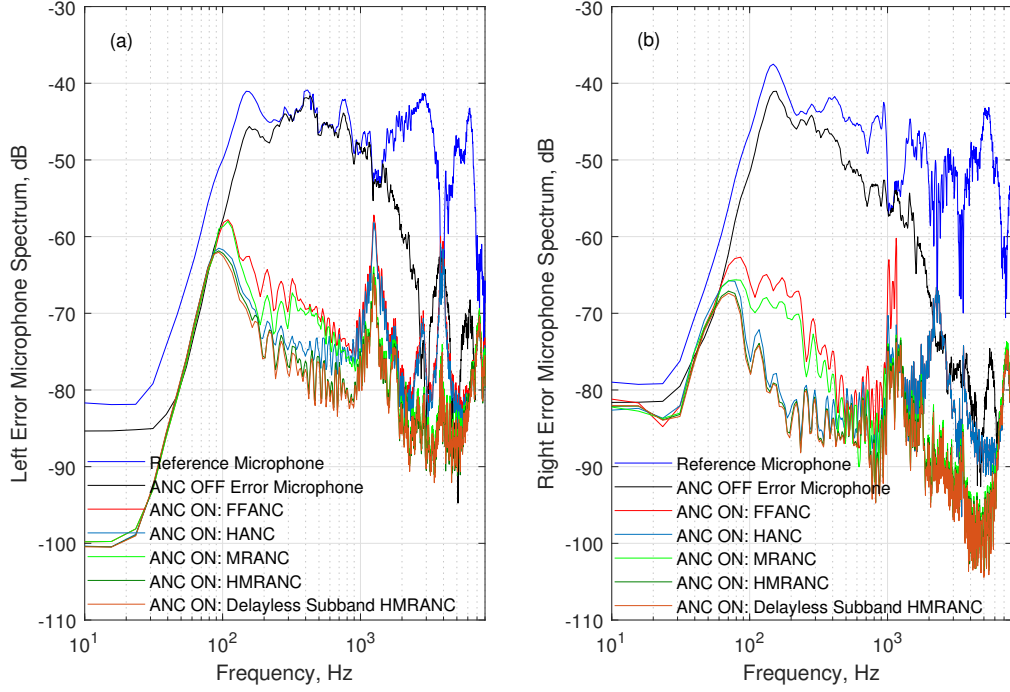


Figure 16: Active attenuation achieved on the left and right error microphone by FFANC, MRANC, HANC, HMRANC and delayless subband HMRANC strategy for noise incident from right side of user.

5. Conclusions

This paper has presented a hybrid multi-reference ANC (HMRANC) headphone system. The proposed HMRANC system is comprised of a feedback controller, implemented using an IMC architecture, and a multi-reference feedforward controller acting simultaneously. The HMRANC headphone system achieves an improved noise attenuation of 5 dB at both the left and right ears compared to the conventional HANC headphone system. In order to reduce the computational burden of HMRANC, a delayless subband version of

the HMRANC headphone system is also presented. It has been demonstrated that the delayless subband HMRANC headphone system is able to achieve the same noise attenuation capability as the HMRANC whilst reducing the computational burden by 40% and increasing the speed of convergence.

Role of the funding source

The work is supported by the Science and Engineering Research Board, Government of India, through the Startup Research Grant Scheme under Grant SRG/2019/001989.

References

- [1] G. W. Evans, M. Bullinger, S. Hygge, Chronic noise exposure and physiological response: A prospective study of children living under environmental stress, *Psychological science* 9 (1) (1998) 75–77.
- [2] C. Hansen, S. Snyder, X. Qiu, L. Brooks, D. Moreau, *Active control of noise and vibration*, CRC press, 2012.
- [3] S. J. Elliott, *Signal Processing for Active Control*, Academic Press, London, 2001.
- [4] M. R. Bai, W. Pan, H. Chen, Active feedforward noise control and signal tracking of headsets: Electroacoustic analysis and system implementation, *The Journal of the Acoustical Society of America* 143 (3) (2018) 1613–1622.

- [5] F. An, Q. Wu, B. Liu, Feedback controller optimization for active noise control headphones considering frequency response mismatch between microphone and human ear, *Applied Sciences* 12 (3) (2022) 977.
- [6] B. Rafaely, Active noise reducing headset-an overview, in: *INTER-NOISE and NOISE-CON Congress and Conference Proceedings*, Vol. 2001, Institute of Noise Control Engineering, 2001, pp. 2144–2153.
- [7] R. Shoureshi, T. Knurek, Automotive applications of a hybrid active noise and vibration control, *IEEE Control Systems Magazine* 16 (6) (1996) 72–78.
- [8] B. Rafaely, M. Jones, Combined feedback–feedforward active noise-reducing headset—the effect of the acoustics on broadband performance, *The Journal of the Acoustical Society of America* 112 (3) (2002) 981–989.
- [9] L. Zhang, X. Qiu, Causality study on a feedforward active noise control headset with different noise coming directions in free field, *Applied Acoustics* 80 (2014) 36–44.
- [10] L. Zhang, J. Tao, X. Qiu, Performance analysis of decentralized multi-channel feedback systems for active noise control in free space, *Applied Acoustics* 74 (1) (2013) 181–188.
- [11] G. Sun, T. Feng, M. Li, T. C. Lim, Convergence analysis of FxLMS-based active noise control for repetitive impulses, *Applied Acoustics* 89 (2015) 178–187.

- [12] J. Chen, J. Yang, A distributed FxLMS algorithm for narrowband active noise control and its convergence analysis, *Journal of Sound and Vibration* 532 (2022) 116986.
- [13] L. E. Ray, J. A. Solbeck, R. D. Collier, Hybrid feedforward-feedback active noise control for hearing protection and communication, Tech. rep., DARTMOUTH COLL HANOVER NH (2005).
- [14] A. D. Streeter, L. R. Ray, R. D. Collier, Hybrid feedforward-feedback active noise control, in: *Proceedings of the 2004 American Control Conference*, Vol. 3, IEEE, 2004, pp. 2876–2881.
- [15] X. Shen, D. Shi, W.-S. Gan, A hybrid approach to combine wireless and earcup microphones for anc headphones with error separation module, in: *ICASSP 2022-2022 IEEE International Conference on Acoustics, Speech and Signal Processing (ICASSP)*, IEEE, 2022, pp. 8702–8706.
- [16] J. Cheer, V. Patel, S. Fontana, The application of a multi-reference control strategy to noise cancelling headphones, *The Journal of the Acoustical Society of America* 145 (5) (2019) 3095–3103.
- [17] V. Belyi, W.-S. Gan, A combined bilateral and binaural active noise control algorithm for closed-back headphones, *Applied Acoustics* 160 (2020) 107129.
- [18] X. Shen, D. Shi, S. Peksi, W.-S. Gan, A multi-channel wireless active noise control headphone with coherence-based weight determination algorithm, *Journal of Signal Processing Systems* (2022) 1–9.

- [19] F. An, B. Liu, Cascade biquad controller design for feedforward active noise control headphones considering incident noise from multiple directions, *Applied Acoustics* 185 (2022) 108430.
- [20] D. Shi, B. Lam, W.-S. Gan, S. Wen, Block coordinate descent based algorithm for computational complexity reduction in multichannel active noise control system, *Mechanical Systems and Signal Processing* 151 (2021) 107346.
- [21] Y. Kajikawa, W.-S. Gan, S. M. Kuo, Recent advances on active noise control: open issues and innovative applications, *APSIPA Transactions on Signal and Information Processing* 1 (2012).
- [22] A. A. Milani, G. Kannan, I. M. Panahi, R. Briggs, Analysis and optimal design of delayless subband active noise control systems for broadband noise, *Signal processing* 90 (4) (2010) 1153–1164.
- [23] D. R. Morgan, J. C. Thi, A delayless subband adaptive filter architecture, *IEEE Transactions on Signal Processing* 43 (8) (1995) 1819–1830.
- [24] A. A. Milani, I. M. S. Panahi, P. C. Loizou, A new delayless subband adaptive filtering algorithm for active noise control systems, *IEEE Transactions on Audio, Speech, and Language Processing* 17 (5) (2009) 1038–1045.
- [25] X. Qiu, N. Li, G. Chen, C. H. Hansen, The implementation of delayless subband active noise control algorithms, in: *Proceedings of the 2006 International Symposium on Active control of Sound and Vibration, 2006*.

- [26] J. Cheer, S. Daley, An investigation of delayless subband adaptive filtering for multi-input multi-output active noise control applications, *IEEE/ACM Transactions on Audio, Speech, and Language Processing* 25 (2) (2017) 359–373.
- [27] D. A. Cartes, L. R. Ray, R. D. Collier, Experimental evaluation of leaky least-mean-square algorithms for active noise reduction in communication headsets, *The Journal of the Acoustical Society of America* 111 (4) (2002) 1758–1771.
- [28] K.-A. Lee, W.-S. Gan, S. M. Kuo, *Subband adaptive filtering: theory and implementation*, John Wiley & Sons, 2009.
- [29] R. Merched, P. S. Diniz, M. R. Petraglia, A new delayless subband adaptive filter structure, *IEEE transactions on signal processing* 47 (6) (1999) 1580–1591.
- [30] S. J. Park, J. H. Yun, Y. C. Park, D. H. Youn, A delayless subband active noise control system for wideband noise control, *IEEE Transactions on Speech and Audio Processing* 9 (8) (2001) 892–899.